The Astrophysical Journal, 872:205 (11pp), 2019 February 20 https://doi.org/10.3847/1538-4357/ab0104

Galactic Rotation and the Oort Constants in the Solar Vicinity

Chengdong Li[1,2], Gang Zhao[1,2], and Chengqun Yang[1,2]
[1] Key Laboratory of Optical Astronomy, National Astronomical Observatories, Chinese Academy of Sciences, Beijing 100012, People's Republic of China
gzhao@nao.cas.cn
[2] School of Astronomy and Space Science, University of Chinese Academy of Sciences, Beijing 100049, People's Republic of China
Received 2018 September 20; revised 2018 December 4; accepted 2019 January 21; published 2019 February 26

Abstract

Gaia DR2 data are used to calculate the Oort constants and derive the Galactic rotational properties in this work. We choose the solar vicinity stars with a "clean" sample within 500 pc. The Oort constants are then fitted through the relation between the proper motions as a function of Galactic longitude l. A maximum likelihood method is adopted to obtain the Oort constants and the uncertainties are produced by a Markov Chain Monte Carlo technique with the sample. Our results for the Oort constants are $A = 15.1 \pm 0.1\,\mathrm{km\,s^{-1}\,kpc^{-1}}$, $B = -13.4 \pm 0.1\,\mathrm{km\,s^{-1}\,kpc^{-1}}$, $C = -2.7 \pm 0.1\,\mathrm{km\,s^{-1}\,kpc^{-1}}$, and $K = -1.7 \pm 0.2\,\mathrm{km\,s^{-1}\,kpc^{-1}}$ respectively. The nonzero values of C and K represent a nonaxisymmetric model for the Galaxy. According to our results, the angular velocity $\Omega = |A - B| = 28.5 \pm 0.1\,\mathrm{km\,s^{-1}\,kpc^{-1}}$ and the circular velocity decreases in solar vicinity. The local radial velocity also decreases along the radial direction due to $C + K$ being negative.

Key words: Galaxy: disk – Galaxy: fundamental parameters – Galaxy: kinematics and dynamics – Galaxy: structure – solar neighborhood

1. Introduction

The stars in the solar vicinity provide an ideal sample to elucidate the structure and evolution of the Galactic disk. The kinematics of stars in the solar neighborhood have been used to explore the properties of the Galactic disk for almost 100 years. Oort pointed out that the local frequency and circular velocity gradient can be represented by the constants from the stream velocity field equation (Oort 1927). He then derived the Oort constants A and B via radial velocities and proper motions and concluded that $A \approx 19\,\mathrm{km\,s^{-1}\,kpc^{-1}}$ and $B \approx -24\,\mathrm{km\,s^{-1}\,kpc^{-1}}$. This result revealed that the Galaxy has a nearly flat rotation curve and ruled out that the Galaxy rotates like a solid body.

Many attempts with various tracers aiming to determine the Oort constants and depict the Galactic rotation have been conducted since then. Kerr & Lynden-Bell (1986) reviewed the previous results and concluded that $A = 14.4 \pm 1.2\,\mathrm{km\,s^{-1}\,kpc^{-1}}$ and $B = -12.0 \pm 2.8\,\mathrm{km\,s^{-1}\,kpc^{-1}}$. Feast & Whitelock (1997) adopted 220 Galactic Cepheids with *Hipparcos* proper motions to obtain that $A = 14.82 \pm 0.84\,\mathrm{km\,s^{-1}\,kpc^{-1}}$ and $B = -12.37 \pm 0.64\,\mathrm{km\,s^{-1}\,kpc^{-1}}$. A similar result was acquired in Metzger et al. (1998) with Cepheids. Tycho-2 catalog stars brighter than $V \sim 11$ were used to derive the Oort constants in Olling & Dehnen (2003). The results are $A \sim 16 \pm 2.8\,\mathrm{km\,s^{-1}\,kpc^{-1}}$ and $B \sim -17 \pm 2.8\,\mathrm{km\,s^{-1}\,kpc^{-1}}$ after correction for the axisymmetric asymmetric-drift effects. Recently, Bovy (2017) used *Gaia* DR1 Tycho-*Gaia* Astrometric Solution main-sequence stars to explore the kinematical patterns of the Galactic disk. The results of Oorts constants are $A = 15.3 \pm 0.4\,\mathrm{km\,s^{-1}\,kpc^{-1}}$, $B = -11.9 \pm 0.4\,\mathrm{km\,s^{-1}\,kpc^{-1}}$, $C = -3.2 \pm 0.4\,\mathrm{km\,s^{-1}\,kpc^{-1}}$, and $K = -3.3 \pm 0.6\,\mathrm{km\,s^{-1}\,kpc^{-1}}$ in this work respectively. The nonzero C and K results show that the velocity field of local stars is nonaxisymmetric and thus reveal a nonaxisymmetry model of the Galaxy (Bovy 2017).

The Oort constants can be related to circular velocity and thus the potential of the Galaxy in an axisymmetric approximation (Binney & Merrifield 1998). The stellar proper motions as a function of Galactic longitude l reveal the relation between the Oort constants and the disk rotational properties. The circular and radial velocity gradients can also be obtained through the Oort constants. As a result, acquiring the Oort constants is beneficial to elucidating the rotational properties of the Galactic disk. *Gaia* DR2 provides an ideal sample to calculate the Oort constants with over 1 billion stars with high precision parallaxes and proper motions. Moreover, the proper motions of *Gaia* are produced on the International Celestial Reference System, which is more reliable for the values of the Oort constants.

We aim to calculate the Oort constants with stars in the solar vicinity in this work and thus select our sample from the *Gaia* DR2 catalog. This paper is organized as follows. In Section 2, we introduce the definition and derived properties of Galactic rotation from the Oort constants. Then we give a brief introduction of *Gaia* DR2 data and present our data selection criteria in Section 3. We calculate the Oort constants and display the results in Section 4. We analyze the rotational properties of Galactic disk revealed from the Oort constants in Section 5. And we finally give a conclusion in Section 6.

2. The Definition and Derivation of the Oort Constants

2.1. Definitions of the Oort Constants

The motions of the stars in the solar vicinity can be decomposed into a streaming velocity and a random motion. In a disk galaxy, the streaming velocity plays a more important role in stellar kinematics. If we make the approximation to ignore the random motions in the coldest limit and assume the Milky Way is axisymmetric, the streaming velocity is then perpendicular to the direction to Galactic center and equal to the circular speed $V_c(R)$ (Binney & Merrifield 1998; Olling & Dehnen 2003). The streaming motions can thus be connected to the potential of the Galaxy.

When we consider a right-handed Cartesian coordinate system centered on the Sun with positive x direction pointing to Galactic center, the streaming velocity of the stars at $\boldsymbol{x} = (x, y)$

can be expanded in a Taylor series by,

$$\boldsymbol{v} = -\boldsymbol{v}_0 + \boldsymbol{H}\cdot\boldsymbol{x} + \mathcal{O}(\boldsymbol{x}^2), \tag{1}$$

where $\boldsymbol{v}_0$ is the velocity of the Sun and

$$\boldsymbol{H} = \begin{pmatrix} \partial v_x/\partial x & \partial v_x/\partial y \\ \partial v_y/\partial x & \partial v_y/\partial y \end{pmatrix} = \begin{pmatrix} K + C & A - B \\ A + B & K - C \end{pmatrix}. \tag{2}$$

The parameters *A, B, C*, and *K* are defined as the Oort constants that represent the four first-order expansion coefficients of the streaming motion with respect to the Sun (Olling & Dehnen 2003).

The Oort constants *A, B, C*, and *K* can also be expressed as follows in cylindrical coordinates with the origin in the Galactic center that can be related to Galactic rotation more clearly

$$\begin{aligned} A &= \frac{1}{2}\left(\frac{v_\varphi}{R} - \frac{\partial v_\varphi}{\partial R} - \frac{1}{R}\frac{\partial v_R}{\partial \varphi}\right) \\ B &= \frac{1}{2}\left(-\frac{v_\varphi}{R} - \frac{\partial v_\varphi}{\partial R} + \frac{1}{R}\frac{\partial v_R}{\partial \varphi}\right) \\ C &= \frac{1}{2}\left(-\frac{v_R}{R} + \frac{\partial v_R}{\partial R} - \frac{1}{R}\frac{\partial v_\varphi}{\partial \varphi}\right) \\ K &= \frac{1}{2}\left(\frac{v_R}{R} + \frac{\partial v_R}{\partial R} + \frac{1}{R}\frac{\partial v_\varphi}{\partial \varphi}\right), \end{aligned} \tag{3}$$

where the v_φ and v_R are mean streaming velocities.

2.2. Derivation of the Oort Constants

In the above four equations, *A* measures the azimuthal shear. If the disk rotates like a solid body, $A = 0$ and thus will vanish. *B* measures the vorticity of the disk, *C* measures the radial shear, and *K* measures the divergence. It should be noted that the Oort constants are related to Galactocentric radius and all four of these parameters can be calculated at a given radius of the disk. Here we only discuss the Oort constants and Galactic rotation in the solar vicinity in this work. The Oort constants also differ in various stellar populations and we will discuss this later in Section 4.

When we consider an axisymmetric model of the Galactic disk, the Oort constants *C* and *K* are equal to zero. As a consequence, the Oort constants in the axisymmetric Galactic model (Binney & Tremaine 2008)

$$A = \frac{1}{2}\left(\frac{v_c}{R} - \frac{\partial v_c}{\partial R}\right) \tag{4}$$

$$B = -\frac{1}{2}\left(\frac{v_c}{R} + \frac{\partial v_c}{\partial R}\right), \tag{5}$$

which coincides with the form given by Oort (1927). Thus the Oort constants can be related with the circular and epicycle frequencies by $\Omega = A - B$ and $\kappa^2 = -4B(A - B)$ (Binney & Tremaine 2008). As a result, if we focus our sight on the solar vicinity, we can get

$$v_c = R_0(A - B) \quad \text{and} \quad \frac{\partial v_c}{\partial R}|_{R_0} = -(A + B), \tag{6}$$

where R_0 denotes the location of the Sun, v_c is the circular velocity of the closed orbit in the solar vicinity, and $\frac{\partial v_c}{\partial R}|_{R_0}$ denotes the slope of the local rotation curve.

However, the real potential of the Galaxy is nonaxisymmetric due to the central bar and the spiral arms in the disk. As a result, the Oort constants *C* and *K* should be nonzero. According to Equation (3), we can obtain

$$\frac{\partial v_R}{\partial R}|_{R_0} = K + C. \tag{7}$$

The measured Oort constants differ from the Oort constants defined in Equation (3) due to the random motions, stars in the high Galactic latitudes, and higher order terms in the Taylor expansion. The spiral arms and central bars change the closed orbit from circular to elliptical and make the measured quantities deviate from the defined Oort constants. The spiral structures raise the level of random motions in the Galactic disk (Sellwood & Carlberg 2014), and the random motions, based on Olling & Dehnen (2003), may generate a systematic disparity from the velocity *v* of closed orbits with the asymmetric drift velocity v_a. On the other hand, the Galactic bar can significantly affect the stellar orbits by trapping the orbits at a resonance with the bar (Binney 2018). The elliptical orbits will visit the resonance from different directions. As a result, the Oort constants tend to show discontinuities when approaching the corotation (CR) or inner-Lindblad resonance and outer-Lindblad resonance (Olling & Dehnen 2003). Due to the Galactic extinction, the Oort constants can be affected by mode mixing when taking the high latitude stars into consideration (Olling & Dehnen 2003). Moreover, the Oort constants in the first order of the streaming velocity field equation can only be used to restrain the Galactic rotation in solar vicinity because the higher order contributions will become significant at large distances (Bovy 2017). For distant stars in the disk, a higher order of the streaming velocity field equation must be taken into consideration (Feast & Whitelock 1997; Siebert et al. 2011).

3. Data Selection

3.1. A Brief Introduction to the Gaia Mission

Gaia is a space-based mission launched by the European Space Agency (ESA) in 2013 December (Gaia Collaboration et al. 2016b). The first data of the *Gaia* mission was released in 2016 September including astrometry and photometry for sources brighter than magnitude 20.7 (Gaia Collaboration et al. 2016a). The second intermediate data of the *Gaia* mission was released on 2018 April 25 and includes over 1 billion sources with high precision parallaxes and proper motions. The typical uncertainty for parallax and proper motion are 0.1 mas and 0.2 mas yr^{-1} for $G = 17$ mag and 0.7 mas and 1.2 mas yr^{-1} for $G = 20$ mag (Gaia Collaboration et al. 2018a). *Gaia* DR2 contains a radial velocity catalog for more than 7 million stars with effective temperature between 3550 and 6900 K (Katz et al. 2018). For the radial velocity, the uncertainty is about 1.4 km s^{-1} for $T_{\mathrm{eff}} = 5000$ K and 3.7 km s^{-1} for $T_{\mathrm{eff}} = 6000$ K at the faint end where $G_{\mathrm{RVS}} = 11.75$ (Katz et al. 2018). *Gaia* DR2 provides photometric parameters for three passbands, *G*, G_{BP}, and G_{RP}. The white-light passband of *G* covers the range 330–1050 nm, the Blue Photometer (BP) and the Red Photometer (RP) cover the wavelength range 330–680 nm and 640–1050 nm respectively (Gaia Collaboration et al. 2016a).

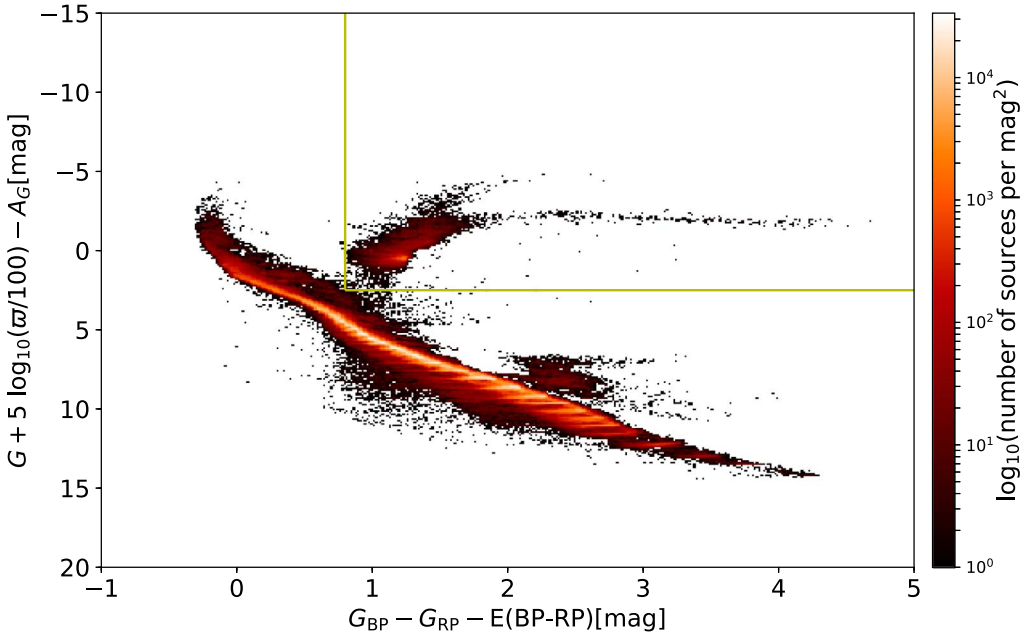

Figure 1. Color–magnitude diagram of our sample stars. The color bar stands for the stellar density and the two lines in this figure separate the main sequence and the red giant branch.

Extinction A_G and color excess $E(\mathrm{BP}-\mathrm{RP})$ are also provided in the *Gaia* DR2 catalog (Andrae et al. 2018).

3.2. Data Selection

Since we mainly focus on the kinematics of the solar vicinity, our sample stars are restricted within $\varpi > 2$ mas and $\varpi/\sigma_\varpi > 10$, where ϖ is the stellar parallax and σ_ϖ denotes the uncertainty of the parallax. The distances are inverted from the parallax directly, that is reasonable approximations and will not introduce additional biases when $\varpi/\sigma_\varpi > 10$ (Bailer-Jones 2015; Luri et al. 2018). Moreover, in order to get a "clean" HR diagram for our sample, we use a modified procedure based on Lindegren et al. (2018) as the following.

The first criteria we use are:

$$\begin{aligned} &\varpi > 2 \text{ mas} \\ &\varpi/\sigma_\varpi > 10 \\ &\text{phot\_BP\_mean\_flux\_over\_error} > 10 \\ &\text{phot\_RP\_mean\_flux\_over\_error} > 10, \end{aligned} \tag{8}$$

which produces more than 10 million stars in total. The last two criteria in Equation (8) restrain the uncertainties in the BP and RP fluxes so that they are less than 10%, correlating to 0.1 mag in G_{BP} and G_{RP} magnitudes. Then we exclude the stars with duplicated_source_flag and phot_variable_flag according to the catalog. After this selection, there are still many stars falling into the unexpected regions between the main sequence and the white dwarf branch. This may be caused by the misidentification of two stars as a single object located in the dense stellar field (Lindegren et al. 2018). Thus the chi-square $\mu = (\chi^2/\nu)^{1/2}$ will increase.

In order to eliminate these stars, we adopt the second criterion as:

$$\mu < 1.2 \times \max(1, \exp(-0.2(G - 19.5))), \tag{9}$$

where μ is obtained by

$$\mu = \sqrt{\text{astrometric\_chi2\_al}/(\text{astrometric\_n\_good\_obs\_al} - 5)}. \tag{10}$$

The last criterion is based on the photometric errors on BP and RP bands that mostly influence the faint stars in crowded fields. The criterion is:

$$\begin{aligned} 1.0 + 0.015 \times (G_{\mathrm{BP}} - G_{\mathrm{RP}})^2 < E < 1.3 + 0.06 \\ \times (G_{\mathrm{BP}} - G_{\mathrm{RP}})^2, \end{aligned} \tag{11}$$

where E is the phot_BP_RP_excess_factor.

In the work of Lindegren et al. (2018), the extinction has been ignored because they use the stars within 100 pc from the Sun. However, we expand this distance to 500 pc in our work. As a result, the extinction should be taken into consideration when we select our "clean" sample.

Only part of the stars in *Gaia* DR2 have extinction A_G and color excess $E(\mathrm{BP}-\mathrm{RP})$ with the consideration of uncertainties in these two parameters. However, the filter in Andrae et al. (2018) will eliminate parts of turn-off stars and lower giant branch stars and produce half of the whole sample with available A_G and $E(\mathrm{BP}-\mathrm{RP})$. The typical uncertainty for A_G and $E(\mathrm{BP}-\mathrm{RP})$ is 0.46 mag and 0.23 mag respectively (Andrae et al. 2018).

We select the stars with available A_G and $E(\mathrm{BP}-\mathrm{RP})$ in our sample to exclude the sources located in the unexpected areas in the color–magnitude diagram. Finally, we exclude the white dwarf branch in our sample. The number of stars in our final sample is 5,391,054 in total. We display the color–magnitude diagram of our sample stars in Figure 1.

4. Measurement of the Oort Constants

4.1. Methods to Calculate the Oort Constants

Although the Oort constants are related with Galactic circular velocity, due to the difficulty in determining the Galactic rotation curve, this relation is more likely used to restrict circular velocity rather than vice versa. One method to constrain the Oort constants is the relation between the Oort constants and line-of-sight velocities of target stellar populations that can be expressed as (Binney & Merrifield 1998):

$$v_{\rm los} = d(K + C\cos 2l + A\sin 2l), \tag{12}$$

where $v_{\rm los}$ denotes the stellar line-of-sight velocity and d is the distance. However, not all the sources in *Gaia* DR2 are provided available line-of-sight velocities and thus will reduce the sample amounts eminently. Here in this work, we calculate the Oort constants through the relation between the Oort constants and stellar proper motions. The stellar proper motion in Galactic coordinates (μ_l, μ_b) can be expressed in the Oort constants and solar motions as follows (Olling & Dehnen 2003),

$$\begin{aligned}\mu_l(l, b, \varpi) = &(A\cos 2l - C\sin 2l + B)\cos b \\ &+ \varpi(u_0\sin l - v_0\cos l),\end{aligned} \tag{13}$$

$$\begin{aligned}\mu_b(l, b, \varpi) = &-(A\sin 2l + C\cos 2l + K)\sin b\cos b \\ &+ \varpi[(u_0\cos l + v_0\sin l)\sin b - w_0\cos b],\end{aligned} \tag{14}$$

where (u_0, v_0, w_0) are the solar motions and azimuthal asymmetric drift with respect to the stellar populations and ϖ is the parallax of the stars.

We use Equations (13) and (14) to constrain the Oort constants according to our sample stars. As a result, the free parameters in the equations are (A, B, C, K, u_0, v_0, w_0). We calculate the proper motion in Galactic coordinates (μ_l, μ_b) based on the observational parameters. Equations (13) and (14) are then used to fit the Oort constants (A, B, C, K).

We convert the proper motion in the equatorial coordinates system to Galactic coordinates. The uncertainties of proper motion in Galactic coordinates are obtained via error propagation from equatorial coordinates. The units of proper motion are converted from mas yr^{-1} to km s^{-1} kpc^{-1} by multiplying 4.74047. We then fit the Equations (13) and (14) based on observational parameters (l, b, ϖ, μ_l, μ_b, err$_{\mu_l}$, err$_{\mu_b}$).

A maximum likelihood method is adopted to fit the best parameters of (A, B, C, K, u_0, v_0, w_0). In order to make the calculation convenient, the likelihood function is always changed into a logarithm form. The log likelihood function with a Gaussian scatter is written as

$$\begin{aligned}\ln\mathcal{L} = -\frac{1}{2}\sum_{i=1}^{N}\Bigg(&\frac{[\mu_l^i - \mu_l(l_i, b_i, \varpi_i)]^2}{\sigma_{\mu_l}^2 + {\rm err}_{\mu_l}^2} - \ln\frac{2\pi}{\sigma_{\mu_l}^2 + {\rm err}_{\mu_l}^2} \\ &+ \frac{[\mu_b^i - \mu_b(l_i, b_i, \varpi_i)]^2}{\sigma_{\mu_b}^2 + {\rm err}_{\mu_b}^2} - \ln\frac{2\pi}{\sigma_{\mu_b}^2 + {\rm err}_{\mu_b}^2}\Bigg),\end{aligned} \tag{15}$$

where σ_{μ_l} and σ_{μ_b} are the Gaussian scatter for the distributions in μ_l and μ_b. The scatter is assumed to be independent with (l, b, ϖ) here that will not impact the best-fit results for free parameters (Bovy 2017). err$_{\mu_l}$ and err$_{\mu_b}$ are the uncertainties in μ_l and μ_b that are acquired through error propagation from μ_α and μ_δ. The uncertainties of the free parameters (A, B, C, K, u_0, v_0, w_0, σ_{μ_l}, σ_{μ_b}) are then obtained via a Markov Chain Monte Carlo (MCMC) technique with emcee code (Foreman-Mackey et al. 2013).

Table 1
Division Principle and Stellar Amounts of Main-sequence Stars

Criteria for Each Color Bin	Number of Stars
$G_{\rm BP} - G_{\rm RP} - E({\rm BP}-{\rm RP}) < 0.8$	767828
$0.8 \leqslant G_{\rm BP} - G_{\rm RP} - E({\rm BP}-{\rm RP}) < 1.2$	1362107
$1.2 \leqslant G_{\rm BP} - G_{\rm RP} - E({\rm BP}-{\rm RP}) < 1.6$	1130427
$1.6 \leqslant G_{\rm BP} - G_{\rm RP} - E({\rm BP}-{\rm RP}) < 2.0$	979819
$2.0 \leqslant G_{\rm BP} - G_{\rm RP} - E({\rm BP}-{\rm RP}) < 2.4$	788811
$G_{\rm BP} - G_{\rm RP} - E({\rm BP}-{\rm RP}) \geqslant 2.4$	324464

4.2. Sample Division

We do not use the sample stars as a whole to calculate the Oort constants in our work. Instead, we divide the stars into several bins and analyze the rotational properties for stellar populations of each bin. Since there are no closed orbits that exist in the Galactic disk, the Oort constants we obtain should indicate the rotational property for the stellar population as our sample and deviate from the closed orbits generated by the Galactic potential. Meanwhile, the young blue stellar populations are not properly dynamical equilibrium because they tend to be affected by the streaming motions and spiral structures in the disk. On the other hand, the old populations such as red giants show more elliptical orbits and larger velocity dispersions. As a consequence, the Oort constants show disparities between various stellar populations.

Trying to analyze this bias, we select a large sample in solar vicinity that holds various stellar populations in Section 3.2. We keep the bluest stars in the main sequence and the red giant branch stars in our sample as is shown in Figure 1. We aim to compare the results of the Oort constants with stars of different populations and obtain more reasonable Oort constants that can indicate the rotational properties in the solar vicinity better.

We divide our sample stars into different populations via the following steps. First, we separate the red giant branch from the main-sequence stars by the crossing lines in Figure 1. There are 37,598 stars belonging to the red giant branch in our sample. For the remaining main-sequence stars, we separate them based on colors minus color excesses $G_{\rm BP} - G_{\rm RP} - E({\rm BP}-{\rm RP})$. The color intervals we used and the amount of stars in each interval are presented in Table 1.

The stellar spatial inhomogeneity distribution of sample stars can lead to biases for the Oort constants (Olling & Dehnen 2003). The completeness of *Gaia* DR2 has improved compared with *Gaia* DR1. The catalog is essentially complete when $12 < G < 17$ (Gaia Collaboration et al. 2018a). We display the distribution of stellar density with Galactic longitude in Figure 2. There are no eminent peaks on either of these color bins in our sample. The bluest color bin shows a differential stellar distribution in Galactic longitude and this trend tends to disappear with the color wandering to the red edge. For the reddest color bin, $G_{\rm BP} - G_{\rm RP} - E({\rm BP}-{\rm RP}) \geqslant 2.4$, the distribution is almost smooth along Galactic longitude and no spatial inhomogeneity exists. In general, the stellar

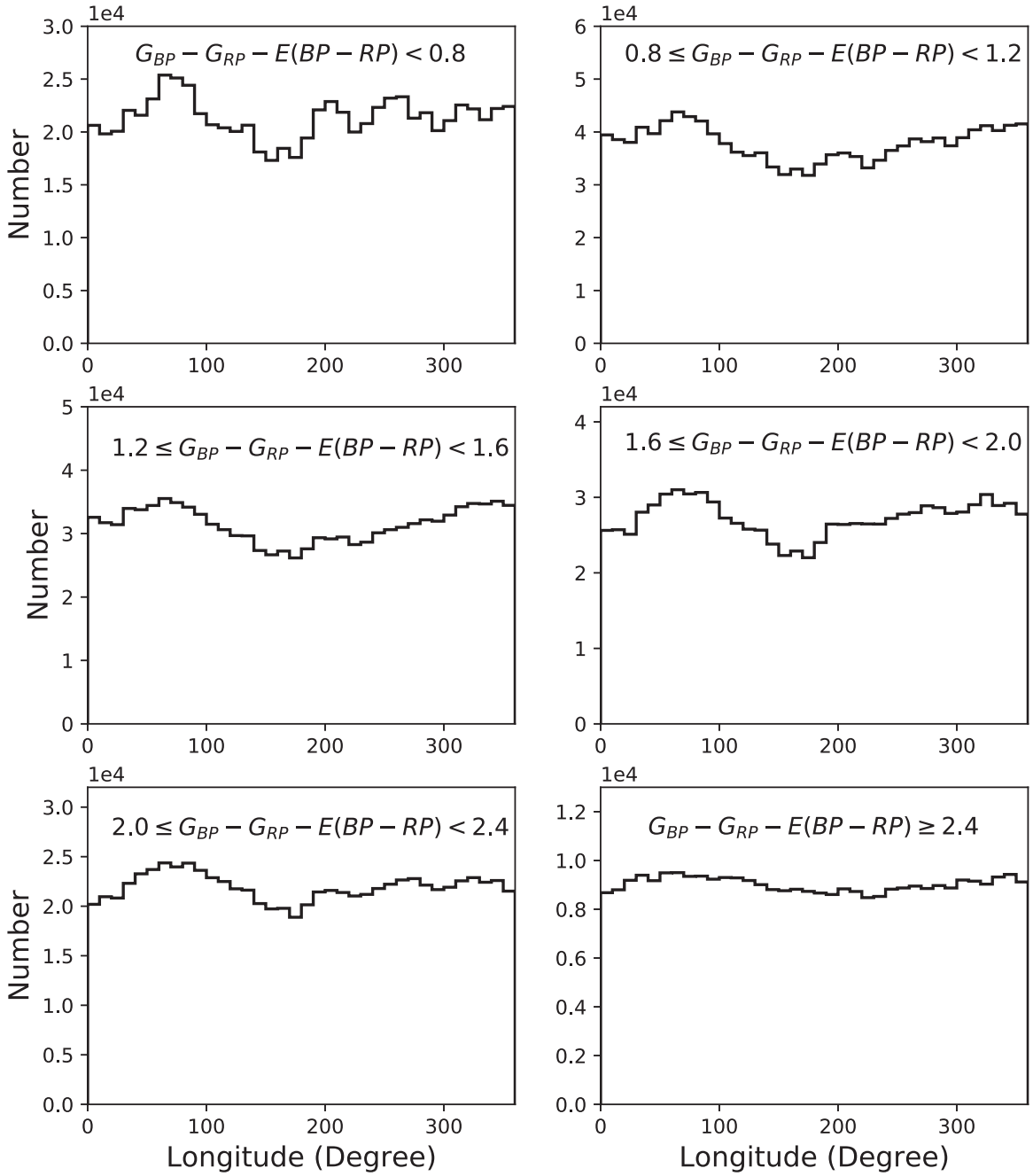

Figure 2. Stellar spatial distribution in each color bin for main-sequence stars in our sample.

density distribution of our sample shows no evident spatial inhomogeneity in each color bin. Thus the bias caused by spatial inhomogeneity that impacts the Oort constants can be avoided in our result.

Except for the spatial inhomogeneity distribution of sample stars, the extinction that affects the magnitude and parallax of the sample stars can also bias the result of the Oort constants. In order to avoid this bias, we only select the stars with convincing extinction and color excess from *Gaia* DR2 as we introduced in Section 3.2. It can reduce the influence on the results of the Oort constants from the extinction.

With the sample stars well divided, we can measure the Oort constants for each color bin in the next stage.

4.3. Results of the Oort Constants for Different Stellar Populations

We use the method described in Section 4.1 to calculate the Oort constants for each color bin in our sample. The free parameters (A, B, C, K, u_0, v_0, w_0, σ_{μ_l}, σ_{μ_b}) are obtained through a maximum likelihood method and the uncertainties are acquired via an MCMC technique. The fit results of the parameters are shown in Figure 3 for $2.0 \leqslant G_{\rm BP} - G_{\rm RP} - E({\rm BP}-{\rm RP}) < 2.4$. We list the Oort constants (A, B, C, K) obtained for red giants and each color bin of main-sequence stars in Table 2. The results of red giants deviate from the main-sequence stars in all the parameters. It indicates that the red giants show obviously diverse kinematical features

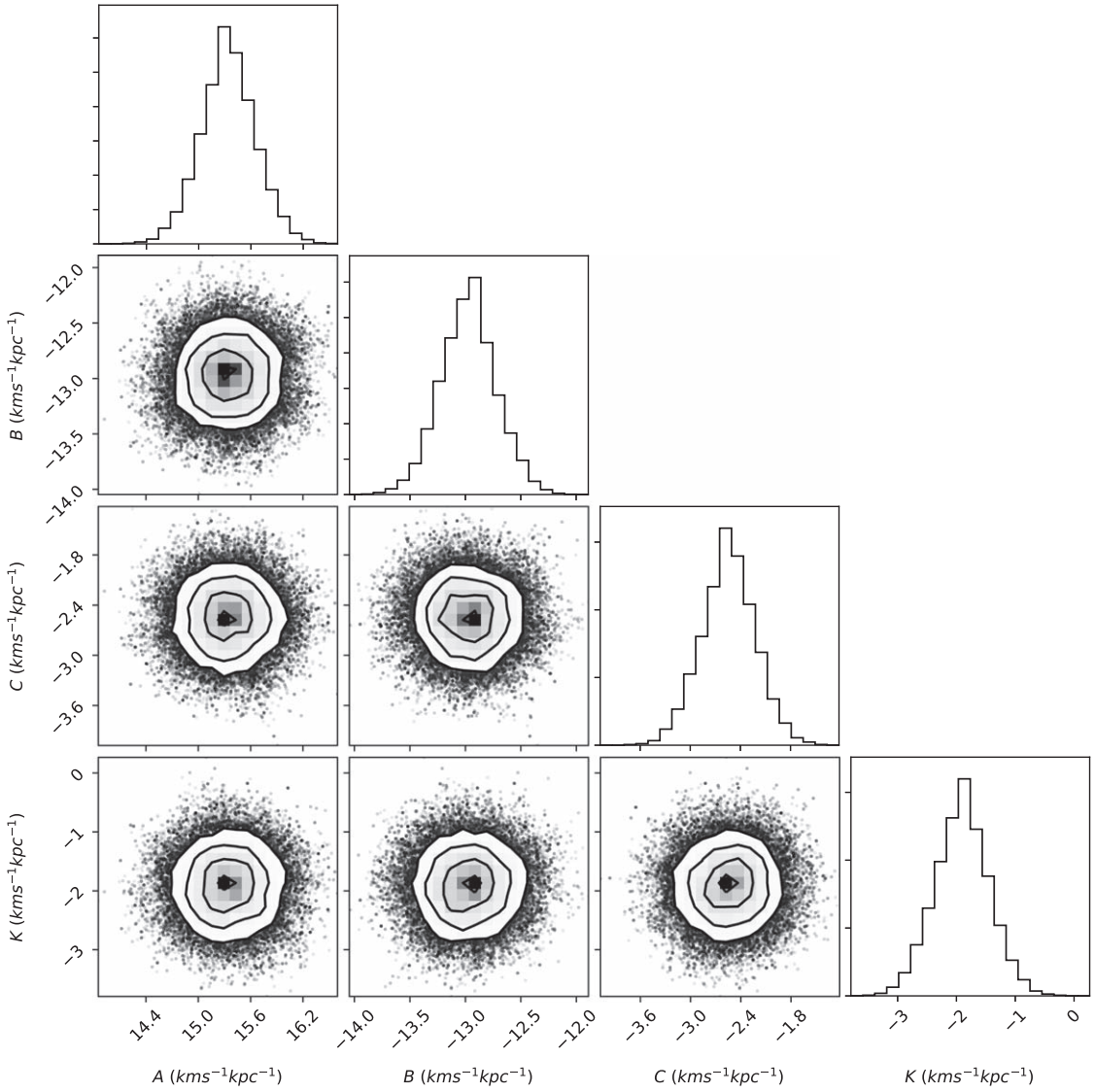

Figure 3. Fit result of the Oort constants (A, B, C, K) for $2.0 \leqslant G_{\rm BP} - G_{\rm RP} - E({\rm BP}-{\rm RP}) < 2.4$.

Table 2
Results of the Oort Constants in Each Color Bin

Bins	A(km s^{-1} kpc^{-1})	B(km s^{-1} kpc^{-1})	C(km s^{-1} kpc^{-1})	K(km s^{-1} kpc^{-1})
$G_{\rm BP} - G_{\rm RP} - E({\rm BP}-{\rm RP}) < 0.8$	15.3 ± 0.2	-13.5 ± 0.2	-3.0 ± 0.2	-2.0 ± 0.3
$0.8 \leqslant G_{\rm BP} - G_{\rm RP} - E({\rm BP}-{\rm RP}) < 1.2$	15.0 ± 0.2	-13.6 ± 0.1	-3.1 ± 0.2	-1.8 ± 0.3
$1.2 \leqslant G_{\rm BP} - G_{\rm RP} - E({\rm BP}-{\rm RP}) < 1.6$	14.9 ± 0.2	-13.4 ± 0.1	-2.6 ± 0.2	-1.7 ± 0.3
$1.6 \leqslant G_{\rm BP} - G_{\rm RP} - E({\rm BP}-{\rm RP}) < 2.0$	15.0 ± 0.2	-13.4 ± 0.2	-2.4 ± 0.2	-1.2 ± 0.4
$2.0 \leqslant G_{\rm BP} - G_{\rm RP} - E({\rm BP}-{\rm RP}) < 2.4$	15.3 ± 0.3	-13.0 ± 0.3	-2.5 ± 0.3	-1.9 ± 0.4
$G_{\rm BP} - G_{\rm RP} - E({\rm BP}-{\rm RP}) \geqslant 2.4$	14.3 ± 0.9	-12.5 ± 0.7	-3.5 ± 0.8	-2.6 ± 1.3
Red giants	17.8 ± 0.8	-11.8 ± 0.6	-4.0 ± 0.8	-3.7 ± 1.2

relative to the main-sequence stars. The lack of red giant stars is another possibility that leads to the result because the filter of the extinctions from *Gaia* DR2 will eliminate some turn-off and lower giant branch stars (Andrae et al. 2018). As a consequence, we do not include the Oort constants of red giants in our final results.

The fit result of μ_l are displayed in Figure 4 for each color bin of main sequence. The observed Galactic longitude proper motions μ_l are corrected for (u_0, v_0, w_0) with respect to each stellar population in this figure as the following equation:

$$\Delta\mu_l = (\mu_l - \varpi(u_0 \sin l - v_0 \cos l))/\cos b. \quad (16)$$

$\Delta\mu_l$ can thus be written as $\Delta\mu_l = A\cos 2l - C\sin 2l + B$ after correction of solar motion. The proper motions μ_l are binned instead of scatter data points in this figure. We only plot the stars with $|b| < 20^\circ$ to show the trend with the consideration of $1/\cos b$ correction. The data points in the last

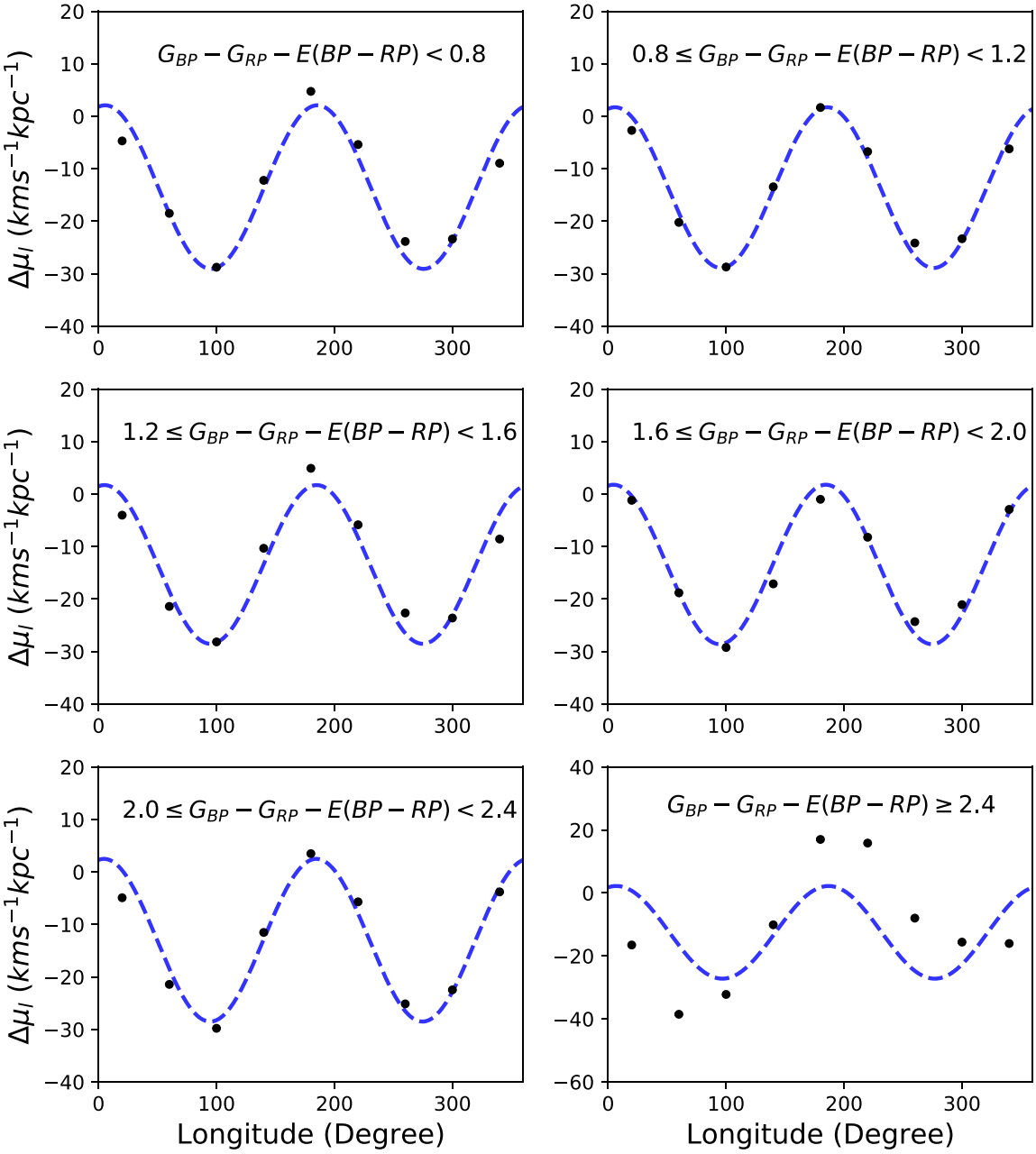

Figure 4. $\Delta\mu_l$ as a function of Galactic longitude l with $|b| < 20°$.

bin show the relative heavy deviation from the model of the proper motions $\Delta\mu_l$ as a function of Galactic longitude l. The results from the first five bins are then used to calculate the final Oort constants in our work.

Similar with μ_l, the fit results of μ_b are displayed in Figure 5 for each color bin. The proper motions in Figure 5 are corrected with (u_0, v_0, w_0) as the following:

$$\Delta\mu_b = -(\mu_b - \varpi((u_0\cos l + v_0\sin l) \times \sin b - w_0\cos b))/(\sin b\cos b). \quad (17)$$

The fit function of $\Delta\mu_b$ is thus $\Delta\mu_b = A\sin 2l + C\cos 2l + K$ after the correction of solar motions. The binned data in this figure are in the interval of $40° < b < 50°$ that aims to display the trend clearly. It is obvious that the data points of the last bin deviate from the model of proper motions again as is shown in Figure 4.

As a conclusion, we use the main-sequence stars to calculate the Oort constants except for the reddest bin. The results for the Oort constants are $A = 15.1 \pm 0.1\ \mathrm{km\,s^{-1}\,kpc^{-1}}$, $B = -13.4 \pm 0.1\ \mathrm{km\,s^{-1}\,kpc^{-1}}$, $C = -2.7 \pm 0.1\ \mathrm{km\,s^{-1}\,kpc^{-1}}$, and $K = -1.7 \pm 0.2\ \mathrm{km\,s^{-1}\,kpc^{-1}}$ respectively.

The free parameters (u_0, v_0, w_0) are shown in Table 3. (u_0, v_0, w_0) are the solar motions and azimuthal asymmetric drift with respect to the stellar populations and $u_0 = u_\odot$, $w_0 = w_\odot$, and $v_0 = v_\odot + v_{a\varphi}$, where $v_{a\varphi}$ is the azimuthal asymmetric drift. The mean values of u and w of our result are $u_\odot = 10.06\ \mathrm{km\,s^{-1}}$ and $w_\odot = 7.93\ \mathrm{km\,s^{-1}}$, which are in accordance with previous results (Dehnen & Binney 1998; Schönrich et al. 2010). The circumstance of v_0 is complicated. v_0 contains two parts, one is the solar motion $v_\odot$, the other is the azimuthal asymmetric drift $v_{a\varphi}$. Based on Figure 2 of Schönrich et al. (2010), the azimuthal asymmetric drift increases from the blue

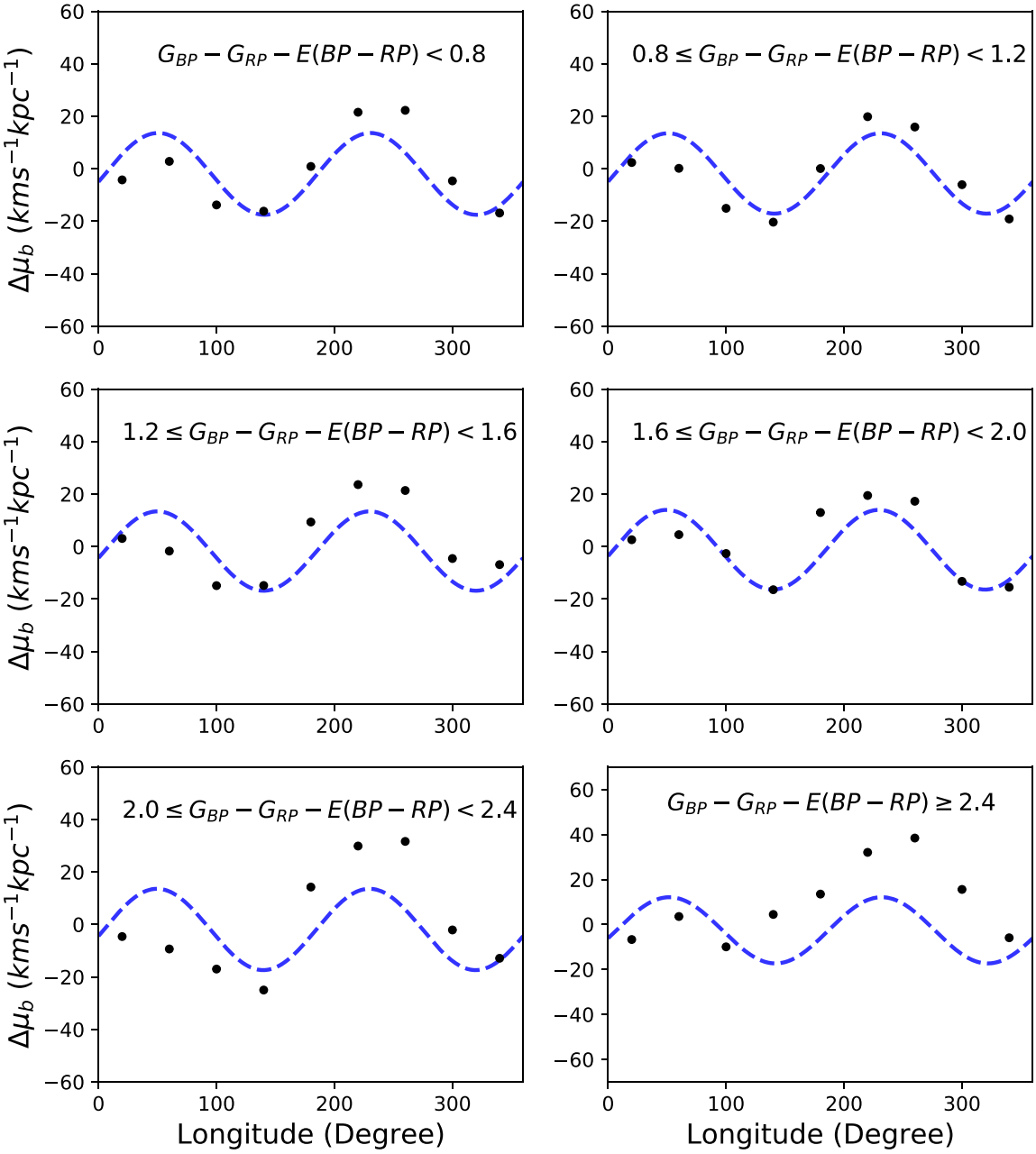

Figure 5. $\Delta\mu_b$ as a function of Galactic longitude l with $40° < b < 50°$.

Table 3
Results of (u_0, v_0, w_0) in Each Color Bin

Bins	u_0(km s^{-1})	v_0(km s^{-1})	w_0(km s^{-1})
$G_{BP} - G_{RP} - E(BP-RP) < 0.8$	9.98 ± 0.04	20.30 ± 0.04	7.51 ± 0.03
$0.8 \leqslant G_{BP} - G_{RP} - E(BP-RP) < 1.2$	10.26 ± 0.04	24.20 ± 0.03	8.32 ± 0.03
$1.2 \leqslant G_{BP} - G_{RP} - E(BP-RP) < 1.6$	10.07 ± 0.04	25.14 ± 0.04	7.92 ± 0.03
$1.6 \leqslant G_{BP} - G_{RP} - E(BP-RP) < 2.0$	10.24 ± 0.05	26.91 ± 0.05	7.92 ± 0.04
$2.0 \leqslant G_{BP} - G_{RP} - E(BP-RP) < 2.4$	9.76 ± 0.05	23.91 ± 0.05	8.00 ± 0.04
$G_{BP} - G_{RP} - E(BP-RP) \geqslant 2.4$	10.41 ± 0.07	22.72 ± 0.06	6.71 ± 0.06
Red giants	9.29 ± 0.20	22.98 ± 0.18	7.75 ± 0.14

end to $B - V = 0.6$ and decreases gradually to the red end. The value of v_0 in our result also shows this trend.

We compare our results of the Oort constants with several previous works in Table 4. The Oort constants A and B have been calculated since Oort (1927). Kerr & Lynden-Bell (1986) summarized the results from previous works and gave the values of $A = 14.4 \pm 1.2$ km s^{-1} kpc^{-1} and $B = -12.0 \pm 2.8$ km s^{-1} kpc^{-1}. Although the observational precisions have

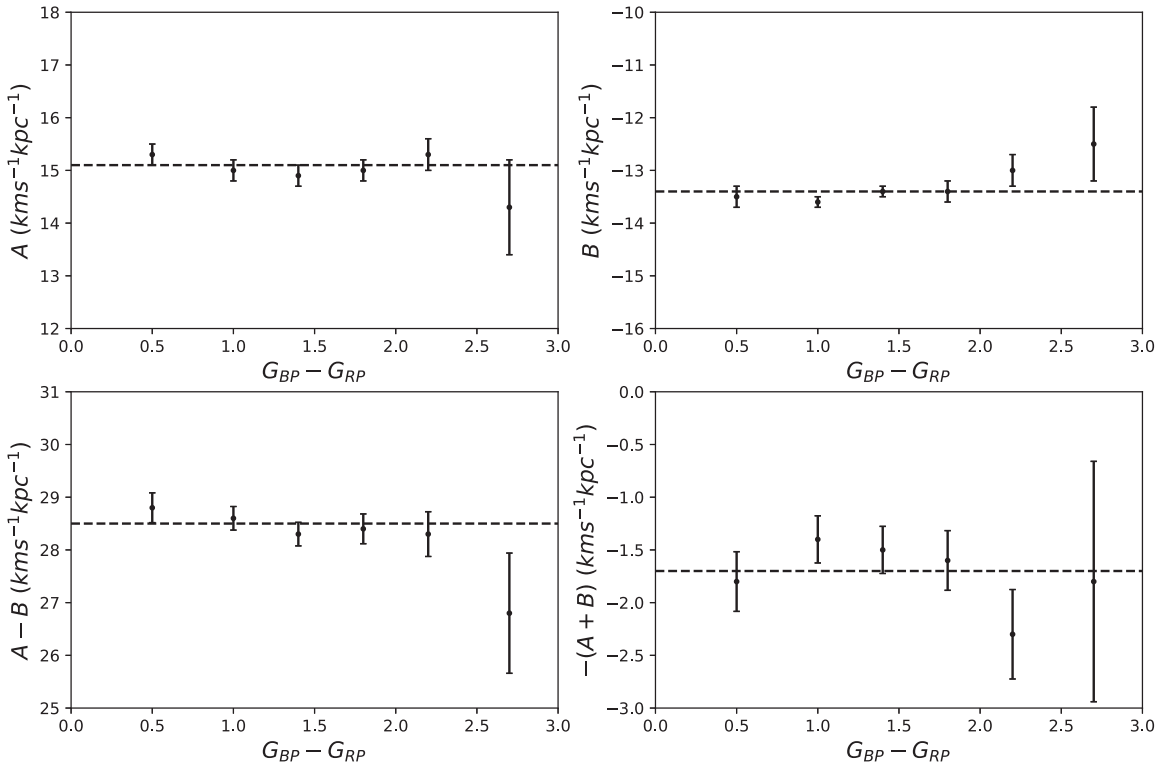

Figure 6. Fit result of the Oort constants A and B for different color bins. The dashed lines denote the values of A, B, $A - B$, and $-(A + B)$.

Table 4
Final Adopted Results of the Oort Constants and Comparison with Previous Works

Origin	A(km s^{-1} kpc^{-1})	B(km s^{-1} kpc^{-1})	C(km s^{-1} kpc^{-1})	K(km s^{-1} kpc^{-1})
Oort (1927)	∼19	∼−24	⋯	⋯
Kerr & Lynden-Bell (1986)	14.4 ± 1.2	−12.0 ± 2.8	⋯	⋯
Comeron et al. (1994)	12.9 ± 0.7	−16.9 ± 1.1	0.4 ± 0.7	−2.1 ± 0.5
Feast & Whitelock (1997)	14.82 ± 0.84	−12.37 ± 0.64	⋯	⋯
Olling & Dehnen (2003)	15.9 ± 2	−16.9 ± 2	−9.8 ± 2	⋯
Bovy (2017)	15.3 ± 0.4	−11.9 ± 0.4	−3.2 ± 0.4	−3.3 ± 0.6
This work	15.1 ± 0.1	−13.4 ± 0.1	−2.7 ± 0.1	−1.7 ± 0.2

been continuously developed since then, the values of A and B are still consistent with the values within uncertainties. However, for the values of C and K, it is another story. Only a few previous works gave the values of C and K. Our result of C shows disparities with the value from Olling & Dehnen (2003) in which $C = -9.8 \pm 2\,\mathrm{km\,s^{-1}\,kpc^{-1}}$. However, their value of $C = -9.8 \pm 2\,\mathrm{km\,s^{-1}\,kpc^{-1}}$ is for the red giant stars in their sample. They also obtained that C for young stars was close to zero and became more negative for older stellar populations (Olling & Dehnen 2003). We obtain both negative values for C and K with approximately $2\,\mathrm{km\,s^{-1}\,kpc^{-1}}$. Our value of C agrees with the computation from Bovy (2015). However, the values of K from this work are closer to zero relative to the results from Bovy (2017). Due to the large amount of stars with high-quality astrometric parameters, the uncertainties of the Oort constants in our work are lower than those in previous works, especially in C and K.

According to Binney & Merrifield (1998) and Olling & Dehnen (2003), the residual systematic rotation of the astrometric reference system can induce the systematic errors and bias the value of Oort constant B heavily. However, in the celestial reference frame of *Gaia* DR2 (Gaia-CRF2), the residual rotation rate is about $\pm 10\,\mu\mathrm{mas\,yr^{-1}}$ (Gaia Collaboration et al. 2018b). This equals approximately $0.05\,\mathrm{km\,s^{-1}\,kpc^{-1}}$, which is much lower than the uncertainty of B in our result. As a conclusion, the systematic error will not bias our result of the Oort constants.

5. Local Galactic Rotational Features from the Oort Constants

Since the Oort constants are related to the coefficients of the streaming velocity field equation, we can derive the local Galactic rotational properties from the Oort constants. We plot the Oort constants A, B, $A - B$, and $-(A + B)$ for each color bin of main-sequence sample stars in Figure 6. It is obvious that the last bin shows deviations from the other five and relatively larger uncertainties. As a consequence, we obtain the Oort constants with the bins except for the reddest one.

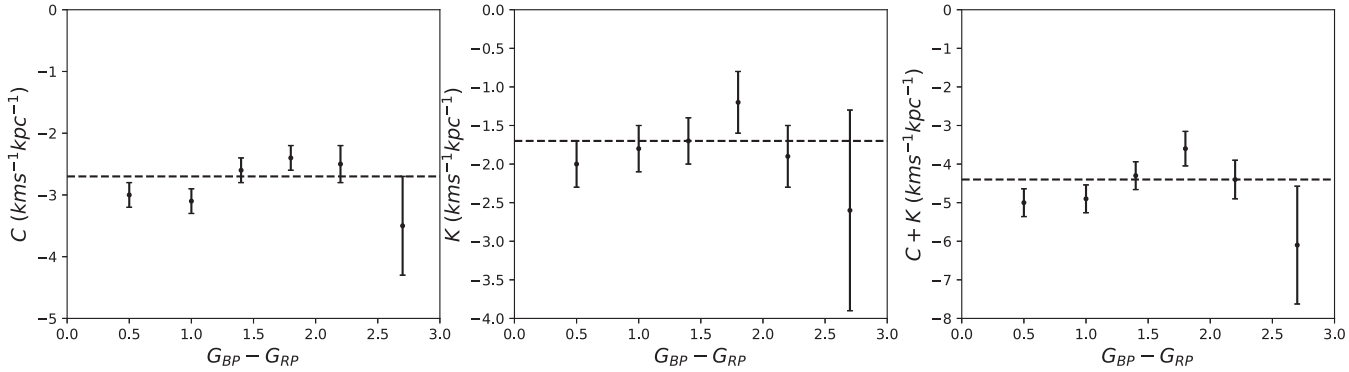

Figure 7. Fit result of the Oort constants C and K for different color bins. The dashed lines denote the values of C, K, and $C + K$.

The local angular velocity can be represented by the Oort constants A and B as $\Omega = |A - B|$. According to our results, $\Omega = |A - B|$ equals $28.5 \pm 0.1\,\mathrm{km\,s^{-1}\,kpc^{-1}}$. This result agrees with the previous works based on the trigonometric parallaxes and proper motions of masers from the star-forming regions and spiral arms of the Galactic disk (Reid et al. 2009, 2014; Bobylev & Bajkova 2010). It also should be noted that the Oort constants cannot be connected to the circular velocity directly due to the nonzero values of C and K. The local gradient of the rotation curve can be denoted as $\frac{\partial v_c}{\partial R}|_{R_0} = -(A + B)$. According to our result, $-(A + B)$ equals $-1.7 \pm 0.1\,\mathrm{km\,s^{-1}\,kpc^{-1}}$. It indicates that the gradient of the rotation curve is negative and the circular velocity decreases in solar vicinity.

The values of C, K, and $C + K$ are displayed in Figure 7. The values of C and K are negative for all the color bins in the main sequence. The nonzero values of C and K indicate the nonaxisymmetric distributions in the solar vicinity. The value of C shows no trend with respect to the colors of various stellar populations, which agrees with the result of Bovy (2017). This is divergent from the simulation result of Minchev & Quillen (2007) in which $|C|$ is larger for the stellar populations with lower velocity dispersions. The local radial velocity gradient can be represented by C and K as $\frac{\partial v_R}{\partial R}|_{R_0} = K + C$. Based on our results, $K + C$ equals $-4.4 \pm 0.2\,\mathrm{km\,s^{-1}\,kpc^{-1}}$. This conclusion agrees with the prediction by Siebert et al. (2011). However, the result of $K + C$ in our work differs from that of Bovy (2017) obtained by TAGS data with a value of $-6.6 \pm 0.7\,\mathrm{km\,s^{-1}\,kpc^{-1}}$.

As we mentioned in Section 4.3, the Oort constants obtained via the RGB sample are not included in the final conclusion. The kinematic properties revealed from RGB stars show prominent diversities from the main-sequence stars. For the RGB stars in our sample, $|A - B|$ equals $29.6 \pm 1.0\,\mathrm{km\,s^{-1}\,kpc^{-1}}$, that represents a larger azimuthal velocity than the main-sequence stars with a larger uncertainty meanwhile. $K + C$ equals $-7.7 \pm 1.4\,\mathrm{km\,s^{-1}\,kpc^{-1}}$ for the RGB stars, which is also larger than that of the main-sequence stars. The larger radial velocity gradient here shows the more prominent change in orbital eccentricity of the older stellar populations relative to the main-sequence stars. However, the number of stars in the RGB sample is much fewer than the other color bins due to the lack of extinction in the *Gaia* DR2 catalog somehow. As a consequence, the value of the Oort constants obtained via RGB stars show larger uncertainties and thus cannot represent the local Oort constants well.

6. Conclusion

We calculate the Oort constants with a large stellar sample in the solar vicinity from *Gaia* DR2 in this work. The number of stars in our sample is 5,391,054 in total. We then allocate the sample stars into different bins via stellar magnitudes and colors. The Oort constants for each bin are then calculated through a maximum likelihood method and the uncertainties are obtained by an MCMC method.

We use the main-sequence stars except for the reddest bin to calculate the final Oort constants. The results are $A = 15.1 \pm 0.1\,\mathrm{km\,s^{-1}\,kpc^{-1}}$, $B = -13.4 \pm 0.1\,\mathrm{km\,s^{-1}\,kpc^{-1}}$, $C = -2.7 \pm 0.1\,\mathrm{km\,s^{-1}\,kpc^{-1}}$, and $K = -1.7 \pm 0.2\,\mathrm{km\,s^{-1}\,kpc^{-1}}$ respectively. The value of $|A - B|$ reveals that the angular velocity Ω equals $28.5 \pm 0.1\,\mathrm{km\,s^{-1}\,kpc^{-1}}$. The gradient of the rotation curve is negative and the circular velocity decreases in solar vicinity based on $-(A + B)$. The nonzero values for C and K indicate that the distribution of the Galactic disk is nonaxisymmetric and the local radial velocity decreases along the radial direction.

We are thankful for the referee's patient perusal and constructive advice that improved this manuscript. C.L. thanks Ji Jiang, Shilong Liao, and Qixun Wang for kind help and discussions. This study is supported by the National Natural Science Foundation of China under grant Nos. 11890694 and 11390371.

This work has made use of data from the European Space Agency (ESA) mission *Gaia* (https://www.cosmos.esa.int/gaia), processed by the *Gaia* Data Processing and Analysis Consortium (DPAC, https://www.cosmos.esa.int/web/gaia/dpac/consortium). Funding for the DPAC has been provided by national institutions, in particular the institutions participating in the *Gaia* Multilateral Agreement.

ORCID iDs

Gang Zhao https://orcid.org/0000-0002-8980-945X
Chengqun Yang https://orcid.org/0000-0003-1972-0086

References

Andrae, R., Fouesneau, M., Creevey, O., et al. 2018, A&A, 616, 8
Bailer-Jones, C. A. L. 2015, PASP, 127, 994
Binney, J. 2018, MNRAS, 474, 2706
Binney, J., & Merrifield, M. 1998, Galactic Astronomy/James Binney and Michael Merrifield (Princeton, NJ: Princeton Univ. Press)
Binney, J., & Tremaine, S. 2008, Galactic Dynamics (2nd ed.; Princeton, NJ: Princeton Univ. Press)
Bobylev, V. V., & Bajkova, A. T. 2010, MNRAS, 408, 1788

Bovy, J. 2015, ApJS, 216, 29
Bovy, J. 2017, MNRAS, 468, L63
Comeron, F., Torra, J., & Gomez, A. E. 1994, A&A, 286, 789
Dehnen, W., & Binney, J. J. 1998, MNRAS, 298, 387
Feast, M., & Whitelock, P. 1997, MNRAS, 291, 683
Foreman-Mackey, D., Hogg, D. W., Lang, D., & Goodman, J. 2013, PASP, 125, 306
Gaia Collaboration, Brown, A. G. A., Vallenari, A., et al. 2016a, A&A, 595, A2
Gaia Collaboration, Brown, A. G. A., Vallenari, A., et al. 2018a, A&A, 616, 1
Gaia Collaboration, Mignard, F., Klioner, S. A., et al. 2018b, A&A, 616, A14
Gaia Collaboration, Prusti, T., de Bruijne, J. H. J., et al. 2016b, A&A, 595, A1
Katz, D., Sartoretti, P., Cropper, M., et al. 2018, arXiv:1804.09372
Kerr, F. J., & Lynden-Bell, D. 1986, MNRAS, 221, 1023
Lindegren, L., Hernandez, J., Bombrun, A., et al. 2018, A&A, 616, 2
Luri, X., Brown, A. G. A., Sarro, L. M., et al. 2018, A&A, 616, A9
Metzger, M. R., Caldwell, J. A. R., & Schechter, P. L. 1998, AJ, 115, 635
Minchev, I., & Quillen, A. C. 2007, MNRAS, 377, 1163
Olling, R. P., & Dehnen, W. 2003, ApJ, 599, 275
Oort, J. H. 1927, BAN, 3, 275
Reid, M. J., Menten, K. M., Brunthaler, A., et al. 2014, ApJ, 783, 130
Reid, M. J., Menten, K. M., Zheng, X. W., et al. 2009, ApJ, 700, 137
Schönrich, R., Binney, J., & Dehnen, W. 2010, MNRAS, 403, 1829
Sellwood, J. A., & Carlberg, R. G. 2014, ApJ, 785, 137
Siebert, A., Famaey, B., Minchev, I., et al. 2011, MNRAS, 412, 2026